Process window estimation in manufacturing through Entropy-Sigma active learning

Jaydeep Karandikar[a,1], Anirban Chaudhuri[b], Scott Smith[a], Tony Schmitz[a,c], Karen Willcox[b]

[a] *Oak Ridge National Laboratory, Oak Ridge, TN*
[b] *University of Texas at Austin, Austin, TX, 78712, USA*
[c] *University of Tennessee, Knoxville, TN, 37996, USA*

Abstract

In manufacturing, there exist boundary identification problems for defining parameter spaces that meet desired thresholds on outcomes. This paper presents an Entropy-Sigma acquisition function for active learning of the process window/map in manufacturing using a Gaussian Process surrogate. The method is applied to identify the stability boundary for the stability process map in machining using time-domain simulations with a periodic sampling stability metric. Results show that the proposed Entropy-Sigma method significantly outperforms Latin hypercube sampling or grid-based methods. The described method can be applied to identify the process window/map for any manufacturing application using a quantitative process outcome metric.

Keywords: contour location, boundary identification, machining, additive manufacturing, stability boundary

1. Introduction

Process boundaries in manufacturing identify the range of process parameters that produce an acceptable behavior for a defined process outcome based on a lower threshold, an upper threshold, or both. The range of process parameters describes a process window or a process map for the specific manufacturing process. The optimal process parameters can be selected from the process window/map that minimizes the total part cost. In laser powder bed fusion (LPBF) additive manufacturing, part porosity can be described as a function of laser power and scan speed [1, 2]. Certain combinations of laser power and scan speed can produce porosity in the part due to lack of fusion [3], keyhole defects [4], or balling up [5, 6]. The combination of lack of fusion, keyhole, and balling up porosity boundaries describe a process window for dense parts, defined by a threshold porosity [1, 7] as illustrated in Fig. 1(a). Similar process windows exist in other additive processes such as electron beam melting (EBM) [8, 9] and wire-feed additive manufacturing [10, 11]. In machining, a stability process map separates stable and unstable (or chatter) combinations of spindle speed and axial depth of cut for a given tool-material combination [12]. Unstable machining can lead to poor surface finish, excessive tool wear, and damage to the tool holder and spindle. A typical stability map is shown in Fig. 1(b) [13].

Estimation of the process window/map is either done using experimentation or process modeling through simulations. The LPBF process has been modeled through finite element methods or high-fidelity mesoscale simulations to identify the process window [14, 15, 16, 17]. Alternatively, experiments can be used to identify the process window for LPBF using a threshold porosity value [18, 19]. For modeling stability process maps in machining, one approach is to complete time domain simulations over the desired grid of spindle speed and axial depth values [20]. The stability at each grid point is decided using a threshold value for a periodic sampling metric calculated from the predicted

[1] Corresponding author. Tel.: +1 8655744641 E-mail address: karandikarjm@ornl.gov (Jaydeep Karandikar).

[2] This manuscript has been authored in part by UT-Battelle, LLC, under contract DE-AC05-00OR22725 with the US Department of Energy (DOE). The US government retains and the publisher, by accepting the article for publication, acknowledges that the US government retains a nonexclusive, paid-up, irrevocable, worldwide license to publish or reproduce the published form of this manuscript, or allow others to do so, for US government purposes. DOE will provide public access to these results of federally sponsored research in accordance with the DOE Public Access Plan (http://energy.gov/downloads/doe-public-access-plan).

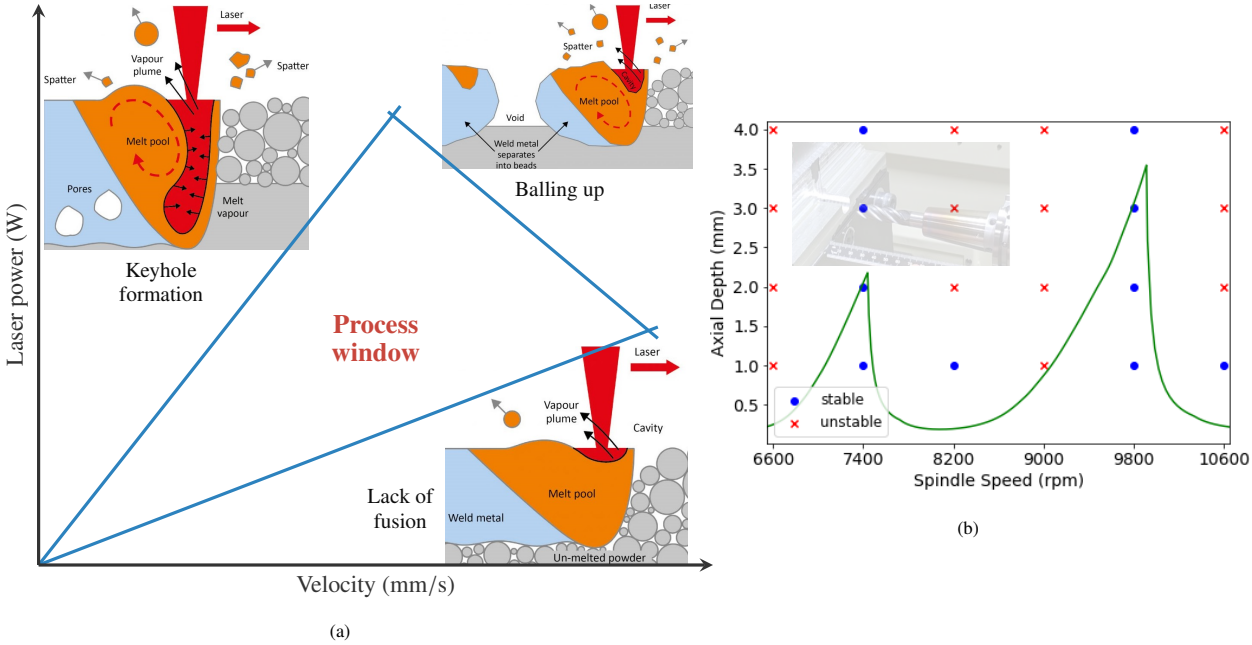

Figure 1: Illustrations showing (a) process window for laser additive manufacturing[3] and (b) stability process map in machining [13]

tool displacements [20]. The simulation or experimental parameters are typically selected using a grid-based or design of experiments (DOE) approach. The DOE and grid-based approaches are inefficient for simulations or physical experiments that can be expensive and time-consuming [21, 22]. This paper presents an entropy-based active learning method for process window/map estimation in manufacturing using minimum number of tests (completed either through simulations or experiments). The goal of this work is to sequentially select the next set of test parameters that provide the most information on the process window/map based on an acquisition function using Gaussian process (GP) surrogates [23]. Much of the efforts in the literature focus on sequential sampling to find the minimum (or maximum) [24, 25]. For the problem of estimating a process window/map, the goal is to identify the process boundary (or contour) that satisfies the defined threshold. There have been a few acquisition functions described in the literature on sequential sampling for boundary identification. Bichon et al. described an expected feasibility function (EFF) that indicates the expectation of the response to be around the feasibility boundary [26] and has been extended to utilize multifidelity models [27]. Other GP-based acquisition functions for failure boundary identification include weighted integrated mean square criterion [28], adaptive Kriging method [29], and population-based adaptive sampling technique [30]. Bect et al. [31] proposed a one-step lookahead strategy for estimating the failure boundary. Marques et al. [32, 33] used an expected change in contour entropy to select the test point in the presence of multiple information sources.

There are two main contributions of the paper. First, this paper presents a novel acquisition function, denoted as Entropy-Sigma, for process window/process map estimation based on the entropy and the prediction uncertainty at the test parameter locations. The Entropy-Sigma acquisition function is computationally inexpensive with a closed-form expression and can be used for identifying process boundaries defined by a lower and an upper threshold as well as for multi-zone windows. Second, the application of the Entropy-Sigma acquisition function method for selecting time-domain simulation parameters for identifying the stability process map in machining is demonstrated. The proposed method is applicable for identifying process window/process map in both additive and subtractive manufacturing.

The remainder of the paper is organized as follows: Section 2 describes the boundary identification problem and the proposed acquisition function for process window/map estimation in manufacturing along with results for two numerical functions. Section 3 describes the application for the selection of time-domain simulation parameters for

[3]The illustrations of defects around the process window are from `https://www.metal-am.com/articles/70927-2/`.

the identification of the stability process map in machining. Conclusions are presented in Section 4.

2. Efficient sampling for process window estimation

This section describes the efficient sampling method for process window/map estimation in manufacturing. The process window estimation problem is described in Section 2.1. Section 2.2 describes the acquisition function and Section 2.3 shows numerical results for two test functions.

2.1. Problem setup

The inputs to the system are m-dimensional parameter vector $z \in \mathcal{Z} \subseteq \mathbb{R}^m$, where $\mathcal{Z}$ denotes the sample space for the input parameters. The process window/map is defined through the system output being lower than a certain threshold, denoted by c. The system output is denoted by $f(z)$, where $f : \mathcal{Z} \mapsto \mathbb{R}$. The process window/map is defined by $f(z) \leq c$, and the boundary is given by the c-contour $f(z) = c$. Note that, without loss of generality, the process window/map can also be reformulated as $f(z) - c \leq 0$, to shift the boundary to the zero-contour. The goal of the work is to efficiently and accurately predict the process window/map through identifying the target process boundary (here, the c-contour) using minimum number of tests.

2.2. Methodology: active learning using Entropy-Sigma

The active learning method uses a computationally inexpensive GP surrogate for approximating $f(z)$. Given a set of n tests, the GP surrogate is fit to the available data $\{z_i, f(z_i)\}_{i=1}^n$. The GP surrogate is updated by sequentially augmenting the data pool with samples based on the GP prediction mean $\mu(z)$ and prediction uncertainty given by the standard deviation $\sigma(z)$. The next test parameter sample, z_{n+1}, to run the test on is selected by maximizing an acquisition function $J(z)$ as $z_{n+1} = \underset{z \in \mathcal{Z}}{\arg\max}\ J(z)$. The process of sequentially adding test parameter samples can be continued until some testing budget is exhausted or a stopping criterion is reached. In this case, the method sequentially selects test parameters to adaptively refine the GP surrogate to learn the process window/process map boundary. In this work, a novel entropy-based acquisition function is defined that considers the trade-off between test parameter locations where the GP prediction mean is close to the threshold (exploitation), and where the GP prediction uncertainty is large (exploration).

For the boundary estimation problem, any test parameter location z has a $P(z)$ probability of being inside the target region (defined by the process window or the process map), $f(z) \leq c$, and a $1 - P(z)$ probability of being outside the target region, $f(z) > c$. The GP prediction at z is the normal distribution $\mathcal{Y}_z \sim \mathcal{N}\left(\mu(z), \sigma^2(z)\right)$. $P(z)$ can be estimated using the GP prediction as

$$P(z) = P[y_z \leq c] = \Phi(\alpha(z)), \tag{1}$$

where y_z is a realization of $\mathcal{Y}_z$, $\alpha(z) = (c - \mu(z))/\sigma(z)$ and $\Phi(.)$ is the standard normal cumulative distribution function. The amount of available information of a discrete random variable with k outcomes occurring with probability $P_i, \ldots, P_k$ can be defined by the entropy $H(P_i, \ldots, P_k) = -\sum_{i=1}^{k} P_i \log(P_i)$ [34]. In this case, any test parameter location z has two discrete outcomes with probabilities $\{P(z), 1 - P(z)\}$ and the entropy is given by

$$H(z) = -\left(P(z)\log(P(z)) + (1 - P(z))\log(1 - P(z))\right). \tag{2}$$

Note that Ref. [32] described an entropy-based approach that uses a change in contour entropy criterion and accounts for multiple information sources but requires numerical approximation. In this work, the proposed approach directly uses the entropy of being above or below the target boundary and has a closed-form solution.

The entropy (or the available information) is maximum at the target boundary when $\mu(z) = c$ with $P(z) = 0.5$. However, all candidate test parameter locations with $\mu(z) = c$ will have the same entropy even if they have different $\sigma(z)$. This is an issue with using the entropy directly as an acquisition function. Ref. [35] proposed an entropy-based method for reliability analysis but the acquisition function does not account for the issue of candidates with $\mu(z) = c$. Intuitively, the parameter set with the higher $\sigma(z)$ is the better candidate and this is built into the acquisition function. The Entropy-Sigma acquisition function, which can distinguish between candidates with $\mu(z) = c$, is defined as the product of the entropy and the prediction uncertainty as

$$J(z) = H(z)\sigma(z). \tag{3}$$

The Entropy-Sigma method can be extended to cases with more than one threshold by creating additional events with their associated probabilities for entropy estimation.

2.3. Numerical tests

The acquisition function was tested using the Branin-Hoo and the modified Matyas test functions [36] with target boundaries defines using thresholds of 50 and 15, respectively. The test functions are given in Appendix A. The Matyas function was modified to mimic the process window for the LPBF process shown in Fig. 1(a). An initial DOE of 4 samples was followed by samples selected using the Entropy-Sigma acquisition function. Fig. 2 shows that the Entropy-Sigma active learning method rapidly convergences to the target boundary within 15 iterations for the Branin function and 10 iterations for the modified Matyas function.

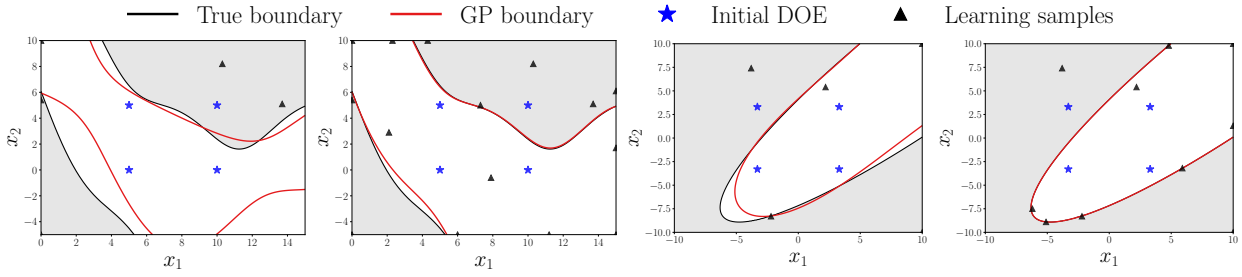

(a) Branin 5 iterations (b) Branin 15 iterations (c) Modified Matyas 5 iterations (d) Modified Matyas 10 iterations

Figure 2: Results for Branin-Hoo and modified Matyas test functions with four initial samples

3. Stability process map in machining

Stability process maps are specific process maps in machining that separate stable and unstable combinations of spindle speed Ω and axial depth b, for a given tool-material combination [12]. One approach for predicting milling stability is through time-domain simulations, which is a numerical solution of the time delay, second-order differential equations of motion in milling [20]. A time-domain simulation can predict the tool displacements and cutting forces in the x (feed) and y directions for a set of machining parameters [12]. The stability limit is determined here using periodic sampling of the predicted tool displacements in the x-direction. The stability metric M is calculated as the average of the sum of the absolute difference of successively once-per-tooth sampled points as [20]

$$M(\Omega, b) = \sum_{i=2}^{N} \frac{|x_d^i(\Omega, b) - x_d^{i-1}(\Omega, b)|}{N}, \tag{4}$$

where x_d is the vector of the once-per-tooth sampled x displacements and N is the length of the x_d vector.

If the simulation parameters are stable, the deviation in the once-per-tooth samples should be zero because the displacement repeats with each tooth passage during forced vibration. If the parameters are unstable, the deviation in the once-per-tooth samples is large because chatter, a self-excited vibration, introduces the new chatter frequency into the solution and the displacement does not repeat from tooth to the next. A threshold value of $c = 1\mu$m is defined here to account for limited numerical precision in the time-domain simulation [20]. The stability process map can be built by completing the time-domain simulations at multiple spindle speed $\Omega \in [6600, 10600]$ rpm and axial depth $b \in [0.1, 4]$ mm combinations and identifying the $M = 1\mu$m contour. To illustrate, Fig. 3(a) shows a map of M as a function of spindle speed and axial depth. The spindle speed and axial depth of cut range were discretized into a grid with intervals of 10 rpm and 0.1 mm, respectively. The time domain simulation was completed at each grid point resulting in 16040 simulations. Fig. 3(a) also shows the predicted stability process map for the $M = 1\mu$m contour. The material, tool geometry, cutting parameters, and the tool-point frequency response function used in the time domain simulation to calculate the stability map shown in Fig. 3 are listed in Ref. [13].

To reduce the number of time domain simulations needed to identify the stability process map, the Entropy-Sigma acquisition function was used to iteratively select the time domain simulation parameters. The stability metric was smoothed to reduce the noise when M is large (> 10) for unstable process parameters (as seen in Fig. 3(a)). The smoothed stability metric M_s is given by

$$M_s(\Omega, b) = s \tanh\left(\frac{M(\Omega, b)}{s}\right). \tag{5}$$

In this work, the value of s is taken as 1. A similar approach was used in Ref. [33]. This ensures that the stability metric is smoothed, reducing the noise in M for unstable parameters. Note that the threshold for the smoothed stability metric to maintain the same boundary is 0.761 since the stability boundary is calculated as $M_s(\Omega, b) = s \tanh(c/s) = 0.761$, where $s = 1$ and $c = 1$. Fig. 3(b) shows the smoothed stability metric. Note that the stability boundary does not change after smoothing as the threshold is modified to 0.761.

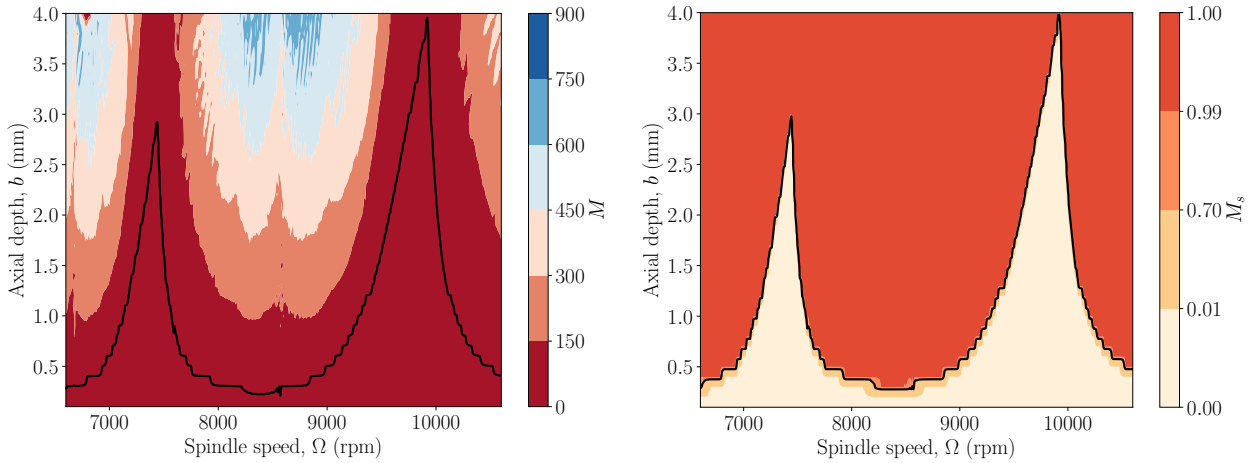

(a) (b)

Figure 3: Stability process map using the time-domain simulation: (a) M contours (b) smoothed M_s contours (black line denotes the stability boundary identified from the grid-based simulations.)

Four initial samples around the center of the (Ω, b) domain were used as the initial design followed by 200 samples selected with the Entropy-Sigma acquisition function. A rational quadratic kernel was used for the GP fit to enable modeling of the sharp corners of the stability process map. Fig. 4(a) and (b) show the results for the Entropy-Sigma acquisition function after 100 samples and 200 samples, respectively. To compare, Fig. 4(c) and (d) show the results for the EFF function [26]. The GP prediction is shown in red and the true stability boundary (using the grid-based simulations in Fig. 3) is shown in black for comparison. Table 1 compares the accuracy for the Entropy-Sigma, EFF, and the Latin hypercube sampling (LHS) method. The accuracy was calculated as the percentage of correctly classified points compared to the true stability process map shown in Fig. 3. The sampling procedure was repeated 100 times for the LHS method and the average accuracy is reported in Table 1. The Entropy-Sigma approach performs similar to the EFF and significantly better than LHS. Note that an advantage of the Entropy-Sigma method over EFF is that the closed-form expression can be applied for for process windows defined by upper and lower threshold as well as multiple zones with different thresholds. The EFF closed-form expression will need to be re-derived (even though the underlying concept remains the same). The Entropy-Sigma active learning results in more than 50% reduction in the number of samples needed to achieve the same accuracy compared to LHS.

4. Conclusions

A GP-based active learning method to identify process boundaries for estimating the process window/map in manufacturing was presented. A new acquisition function, Entropy-Sigma, that considers the entropy of a test parameter

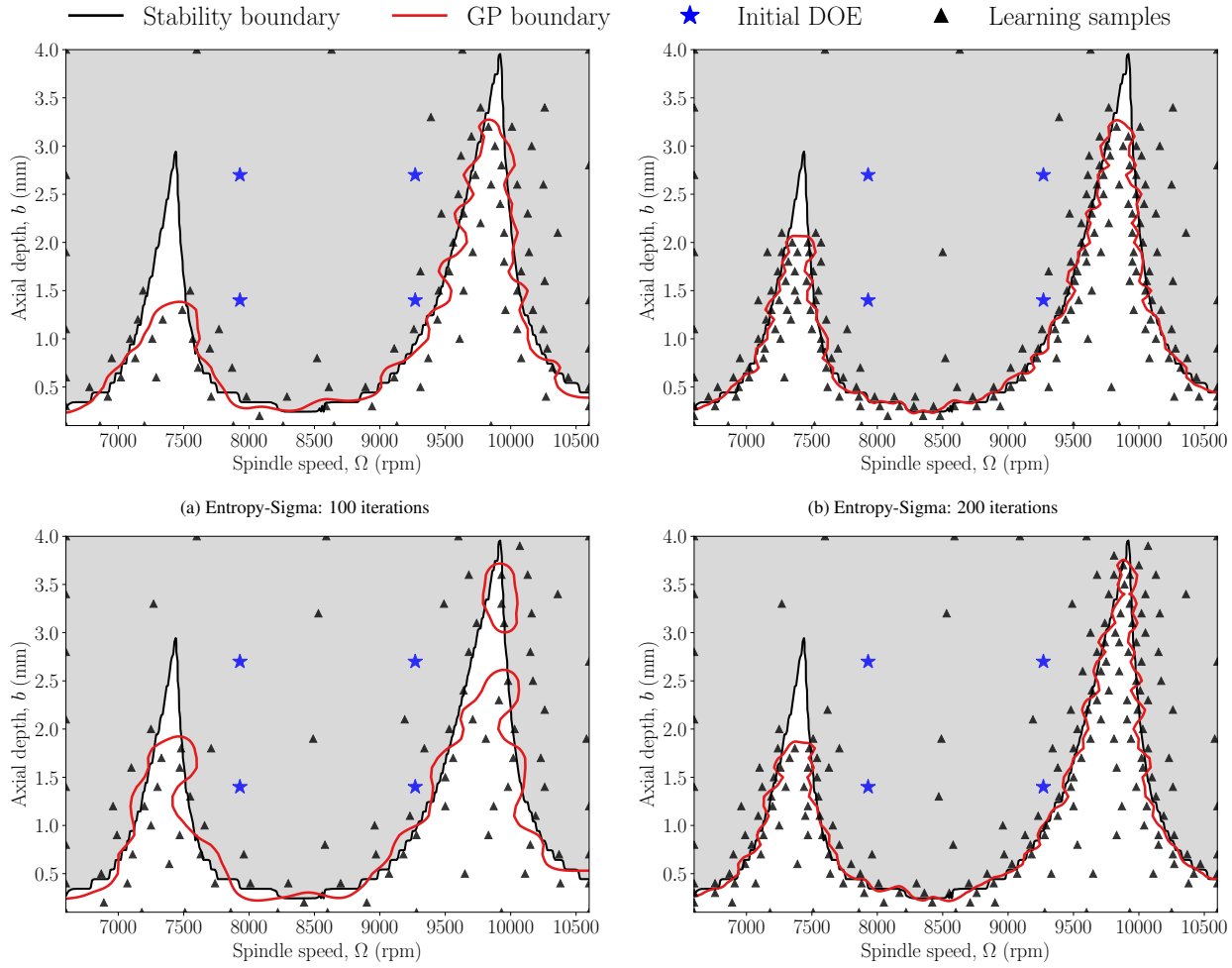

(a) Entropy-Sigma: 100 iterations

(b) Entropy-Sigma: 200 iterations

(c) EFF: 100 iterations

(d) EFF: 200 iterations

Figure 4: Results from iterative sampling for stability process map identification starting using with the Entropy-Sigma acquisition function and EFF after 100 simulations and 200 simulations.

Table 1: Accuracy for Entropy-Sigma, EFF, and LHS method for different iterations.

Iterations	Entropy-Sigma	EFF	LHS
50	92.23	93.65	87.32
100	95.60	94.66	91.1
150	97.24	96.68	93.54
200	97.57	97.52	94.00

along with the prediction uncertainty to balance the trade-off between exploration and exploitation was described. Results on numerical functions showed a rapid convergence to the true boundary. The method was applied for stability process map identification in machining using time domain simulations. Results showed more than 50% decrease in the number of time-domain simulations needed to identify the stability process map compared to the LHS method. The Entropy-Sigma acquisition function has the following advantages. First, it is computationally inexpensive and has a closed-form expression. Second, the method can be applied for process windows defined by a lower threshold, an upper threshold, or a combination of both. Third, the method can be easily extended to identify multiple zones in a process window with different thresholds.

Acknowledgements

This work has been supported in part by the DOE Office of Energy Efficiency and Renewable Energy (EERE), Manufacturing Science Division, and used resources at the Manufacturing Demonstration Facility, a DOE-EERE User Facility at Oak Ridge National Laboratory. The second and last authors acknowledge support from Department of Energy award number DE-SC0021239 and ARPA-E Differentiate award number DE-AR0001208.

Appendix A. Numerical functions for algorithm testing

The Branin-Hoo function is given by

$$f(x) = a(x_2 - bx_1^2 + cx_1 - r)^2 + s(1-t)cos(x_1) + s, \tag{A.1}$$

where $a = 1, b = 5.1/(4\pi^2), c = 5/\pi, r = 6, s = 10$, and $t = 1/(8\pi)$.

The modified Matyas function is given by

$$f(x) = 0.26(x_1^2 + x_2^2) - 0.48x_1x_2 - 1.8x_1 + 7.3845. \tag{A.2}$$

References

[1] H. Gong, K. Rafi, H. Gu, T. Starr, B. Stucker, Analysis of defect generation in ti–6al–4v parts made using powder bed fusion additive manufacturing processes, Additive Manufacturing 1 (2014) 87–98.
[2] H. Choo, K.-L. Sham, J. Bohling, A. Ngo, X. Xiao, Y. Ren, P. J. Depond, M. J. Matthews, E. Garlea, Effect of laser power on defect, texture, and microstructure of a laser powder bed fusion processed 316l stainless steel, Materials & Design 164 (2019) 107534.
[3] M. Tang, P. C. Pistorius, J. L. Beuth, Prediction of lack-of-fusion porosity for powder bed fusion, Additive Manufacturing 14 (2017) 39–48.
[4] R. Cunningham, C. Zhao, N. Parab, C. Kantzos, J. Pauza, K. Fezzaa, T. Sun, A. D. Rollett, Keyhole threshold and morphology in laser melting revealed by ultrahigh-speed x-ray imaging, Science 363 (6429) (2019) 849–852.
[5] R. Li, J. Liu, Y. Shi, L. Wang, W. Jiang, Balling behavior of stainless steel and nickel powder during selective laser melting process, The International Journal of Advanced Manufacturing Technology 59 (9) (2012) 1025–1035.
[6] D. Gu, Y. Shen, Balling phenomena during direct laser sintering of multi-component cu-based metal powder, Journal of Alloys and Compounds 432 (1-2) (2007) 163–166.
[7] J. V. Gordon, S. P. Narra, R. W. Cunningham, H. Liu, H. Chen, R. M. Suter, J. L. Beuth, A. D. Rollett, Defect structure process maps for laser powder bed fusion additive manufacturing, Additive Manufacturing 36 (2020) 101552.
[8] V. Juechter, T. Scharowsky, R. Singer, C. Körner, Processing window and evaporation phenomena for ti–6al–4v produced by selective electron beam melting, Acta Materialia 76 (2014) 252–258.
[9] M. F. Zäh, S. Lutzmann, Modelling and simulation of electron beam melting, Production Engineering 4 (1) (2010) 15–23.
[10] Z. Nie, G. Wang, J. D. McGuffin-Cawley, B. Narayanan, S. Zhang, D. Schwam, M. Kottman, Y. K. Rong, Experimental study and modeling of h13 steel deposition using laser hot-wire additive manufacturing, Journal of Materials Processing Technology 235 (2016) 171–186.
[11] L. Sun, F. Jiang, R. Huang, D. Yuan, Y. Su, C. Guo, J. Wang, Investigation on the process window with liner energy density for single-layer parts fabricated by wire and arc additive manufacturing, Journal of Manufacturing Processes 56 (2020) 898–907.
[12] T. L. Schmitz, K. S. Smith, Machining dynamics, Springer, 2014.
[13] J. Karandikar, A. Honeycutt, T. Schmitz, S. Smith, Stability boundary and optimal operating parameter identification in milling using bayesian learning, Journal of Manufacturing Processes 56 (2020) 1252–1262.
[14] M. Masoomi, S. M. Thompson, N. Shamsaei, Laser powder bed fusion of ti-6al-4v parts: Thermal modeling and mechanical implications, International Journal of Machine Tools and Manufacture 118 (2017) 73–90.
[15] D. S. Nakapkin, A. V. Zakirov, S. A. Belousov, M. V. Bogdanova, B. A. Korneev, A. E. Stepanov, A. Y. Perepelkina, V. D. Levchenko, B. V. Potapkin, A. Meshkov, Finding optimal parameter ranges for laser powder bed fusion with predictive modeling at mesoscale, in: Sim-AM 2019: II International Conference on Simulation for Additive Manufacturing, CIMNE, 2019, pp. 297–308.
[16] A. J. Dunbar, E. R. Denlinger, M. F. Gouge, P. Michaleris, Experimental validation of finite element modeling for laser powder bed fusion deformation, Additive Manufacturing 12 (2016) 108–120.
[17] A. Zakirov, S. Belousov, M. Bogdanova, B. Korneev, A. Stepanov, A. Perepelkina, V. Levchenko, A. Meshkov, B. Potapkin, Predictive modeling of laser and electron beam powder bed fusion additive manufacturing of metals at the mesoscale, Additive Manufacturing 35 (2020) 101236.
[18] K. Aoyagi, H. Wang, H. Sudo, A. Chiba, Simple method to construct process maps for additive manufacturing using a support vector machine, Additive Manufacturing 27 (2019) 353–362.
[19] G. Tapia, S. Khairallah, M. Matthews, W. E. King, A. Elwany, Gaussian process-based surrogate modeling framework for process planning in laser powder-bed fusion additive manufacturing of 316l stainless steel, The International Journal of Advanced Manufacturing Technology 94 (9) (2018) 3591–3603.
[20] A. Honeycutt, T. L. Schmitz, A new metric for automated stability identification in time domain milling simulation, Journal of Manufacturing Science and Engineering 138 (7) (2016).

[21] C. Wang, X. Tan, S. Tor, C. Lim, Machine learning in additive manufacturing: State-of-the-art and perspectives, Additive Manufacturing (2020) 101538.
[22] L. Meng, B. McWilliams, W. Jarosinski, H.-Y. Park, Y.-G. Jung, J. Lee, J. Zhang, Machine learning in additive manufacturing: A review, Jom 72 (6) (2020) 2363–2377.
[23] C. E. Rasmussen, Gaussian processes in machine learning, in: Summer school on machine learning, Springer, 2003, pp. 63–71.
[24] D. R. Jones, A taxonomy of global optimization methods based on response surfaces, Journal of global optimization 21 (4) (2001) 345–383.
[25] A. I. Forrester, A. J. Keane, Recent advances in surrogate-based optimization, Progress in aerospace sciences 45 (1-3) (2009) 50–79.
[26] B. J. Bichon, M. S. Eldred, S. Mahadevan, J. M. McFarland, Efficient global surrogate modeling for reliability-based design optimization, Journal of Mechanical Design 135 (1) (2013).
[27] A. Chaudhuri, A. N. Marques, K. Willcox, mfegra: Multifidelity efficient global reliability analysis through active learning for failure boundary location, Structural and Multidisciplinary Optimization 64 (2) (2021) 797–811.
[28] V. Picheny, D. Ginsbourger, O. Roustant, R. T. Haftka, N.-H. Kim, Adaptive designs of experiments for accurate approximation of a target region, Journal of Mechanical Design 132 (7) (2010) 071008.
[29] B. Echard, N. Gayton, M. Lemaire, AK-MCS: an active learning reliability method combining kriging and monte carlo simulation, Structural Safety 33 (2) (2011) 145–154.
[30] V. Dubourg, B. Sudret, J.-M. Bourinet, Reliability-based design optimization using kriging surrogates and subset simulation, Structural and Multidisciplinary Optimization 44 (5) (2011) 673–690.
[31] J. Bect, D. Ginsbourger, L. Li, V. Picheny, E. Vazquez, Sequential design of computer experiments for the estimation of a probability of failure, Statistics and Computing 22 (3) (2012) 773–793.
[32] A. Marques, R. Lam, K. Willcox, Contour location via entropy reduction leveraging multiple information sources, Advances in neural information processing systems 31 (2018).
[33] A. N. Marques, M. M. Opgenoord, R. R. Lam, A. Chaudhuri, K. E. Willcox, Multifidelity method for locating aeroelastic flutter boundaries, AIAA Journal 58 (4) (2020) 1772–1784.
[34] R. M. Gray, Entropy and information theory, Springer Science & Business Media, 2011.
[35] D. A. Cole, R. B. Gramacy, J. E. Warner, G. F. Bomarito, P. E. Leser, W. P. Leser, Entropy-based adaptive design for contour finding and estimating reliability, arXiv preprint arXiv:2105.11357 (2021).
[36] Optimization test functions and datasets, `https://www.sfu.ca/~ssurjano/optimization.html`, accessed: 06-01-2021.